Indian Journal of Pure & Applied Physics
Vol. 55, August 2017, pp. 589-594

Electron momentum density and band structure calculations of Dy_2O_3

Gagan Ahuja[a], Sonu Sharma[b] & Gunjan Arora[c]*

[a]Department of Physics, Faculty of Science, Pacific Academy of Higher Education and Research University, Udaipur 313 022, India

[b]Department of Physics, College of Science, M L Sukhadia University, Udaipur 313 001, India

[c]Department of Physics, Geetanjali Institute of Technical Studies, Udaipur 313 022, India

Received 8 March 2017; accepted 26 April 2017

The electronic properties of dysprosium sesquioxide have been investigated (Dy_2O_3) by employing the linear combination of atomic orbitals method within the framework of density functional theory. The energy bands, density of states, isotropic and anisotropic Compton profiles and Mulliken's populations of Dy_2O_3 have been computed. Theoretical anisotropies in Compton profile along [100], [110] and [111] directions have been explained in terms of energy bands. Results of the present calculations have been compared with previous experimental measurements and calculations.

Keywords : Band structure calculations, Density functional theory, Electron momentum density, Rare earth oxides

1 Introduction

The rare earth oxides have been extensively investigated due to their important applications as catalysts[1], catalyst support, dopants for lasers, materials for magneto optic memory and colorants for special glasses. Due to large band gap characteristics (≈ 4.9 eV) they have wide range of technological applications including memory devices, switching mechanism for logic devices, and optoelectronic devices[2]. These oxides are also found as potential candidates of metal oxide semiconductor devices[3]. Dysprosium sesquioxide (Dy_2O_3) has dielectric constant in the range of 14-18, which is higher than that of SiO_2 (i.e., 3.9), so it has application in high dielectric constant gate oxides[4]; also, it substitutes SiO_2 in the CMOS devices as its dielectric constant and chemical and thermal stability with Si is high[5]. Dy_2O_3 is useful for corrosion resistive coating as it is thermodynamic stable[6,7]. Dy_2O_3 leads to application in optics, such as antireflection coatings, switches, filters and modulators[8] because of its high refractive index, 1.976. Crystal structure of the trivalent sesquioxides (Ln_2O_3) fall into three distinct polymorphic forms cubic Ia3, hexagonal P-3m1 and monoclinic C2/m, while the tetravalent fall into cubic Fm3m[9].

Recently, Han *et al.*[10] have performed a controlled study of substrate surface modifications with nano-sized second-phase pre-formed Dy_2O_3 to get improved critical current density in $Y_{0.5}Gd_{0.5}Ba_2Cu_3O_x$ thin films. Horoz *et al.*[11] have investigated the electronic and optical properties of Dy_2O_3 using the density functional theory (DFT) within the generalized gradiant approximation (GGA) by using Vienna *ab intio* simulation program (VASP). Chandrasekhar *et al.*[12] have compared the structural and luminescence properties of Dy_2O_3 nanopowders synthesized by co-precipitation and green combustion routes. Electric structure of lanthanides (Ln_2O_3 and CeO_2) has been calculated by Gillen *et al.*[13] using hybrid density functional HSE03, HSE06 and screened exchange. Zelati *et al.*[14] have manufactured and characterized Dy_2O_3 nanoparticles by using combustion method, X-ray diffraction, transmission electron microscopy and photoluminescence. Electronic properties of lanthanide sesquioxides have been reported by Jiang *et al.*[15] using GW calculations on Hubbard U corrected local density approximation (LDA) approach. Rammo[16] has studied a number of Ln_xO_y rare-earth oxides by powder diffractometry and pycnometry coupled with the simulation of their lattice dimensions by empirically derived pair potentials using the GULP code. Dilawr *et al.*[17] have used Raman spectroscopy to study the variation in vibrational spectra of a series of rare earth sesquioxides of composition Ln_2O_3 (where Ln= Y, Sm, Eu, Gd, Dy, Ho, Er and Yb) which were also characterized by using X-ray diffraction and Atomic Force Microscopy. Chiu[18] has studied the electrical characterisation and current transportation in metal/Dy_2O_3/Si structure. The electronic structures of dioxides, REO_2, and sesquioxides, RE_2O_3, of the

*Corresponding author (E-mail: garora.gits@gmail.com)

rare earths, have been calculated by Petit *et al.*[19] with the self-interaction-corrected local-spin-density approximation. Medenbach *et al.*[20] have reported the refractive index and optical dispersion of rare earth oxides using small-prism technique. Prokofiev *et al.*[21] have used photo absorption method to determine the periodicity in band gap variation in rare earth oxides. Using the adsorption of electron acceptors on metal oxides Sugunan *et al.*[22] have explored the electron donor properties of Dy_2O_3.

The properties and the functionality of materials are determined to a large extent by their electronic structure. The electronic structure can be examined through the electron momentum density (EMD), which is classically equivalent to the velocity distribution of the electrons. Changes in the structure of materials induce changes on their electronic structure, which in turn are reflected as changes in the EMDs that can be routinely measured using, e.g., X-ray compton scattering.

To the best of our knowledge, EMD of Dy_2O_3 is still unexplored. In this paper, we report theoretical directional and isotropic valence Compton profile (CPs) using DFT within the linear combination of atomic orbitals (LCAO) scheme. Further, we have also computed the energy bands, partial and total density of states (DOS), band gap and charge reorganization using Mulliken's population (MP) analysis.

2 Computational Method

The electronic structure (including momentum densities) of Dy_2O_3 has been computed using self-consistent pseudopotential (PP) band structure calculations embodied in CRYSTAL09 package of Torino group[23, 24]. Within the PP prescription, the code facilitates various schemes namely HF, DFT with LDA and GGA; and also *posteriori* Becke's three parameter hybrid functional (viz. B3LYP). The present computations have been carried out by using the pseudopotential (PP) approach. In PP-Hartree-Fock (HF) scheme, the one electron Hamiltonian operator is given by[23]:

$$\hat{h}_{\mathrm{PP}} = \hat{t} + \hat{c} + \hat{x}_{\mathrm{HF}} + \hat{e}_{\mathrm{PP}} \quad \ldots (1)$$

where $\hat{t}$, $\hat{c}$, $\hat{x}_{\mathrm{HF}}$ and $\hat{e}_{\mathrm{PP}}$ are kinetic, Coulomb, exchange and effective core pseudopotential (ECP) operators, respectively. For the present computations, we have incorporated DFT-PP-LDA, DFT-PP-WCGGA DFT-PP-PBEsol, DFT-PP-SOGGA and PP-B3LYP calculations. A hybrid DFT–HF method, so-called B3LYP, was employed by 20% mixing of the HF matrix with the DFT matrix. Different exchange and correlation functionals used in the present work are mentioned in Table 1. The ECP was used to describe the core part of Dy[32] while the all electron basis sets[33] were taken for O. The lattice parameter for cubic Dy_2O_3 was taken[16] as a = 10.665 Å. The density functional exchange-correlation contribution is evaluated by numerical integration over the unit cell volume.

3 Results and Discussion

3.1 Energy bands and density of states

In Fig. 1(a, b), we have plotted the energy bands and DOS (with E_F shifted to zero reference level) along the high-symmetry directions of brillouin zone for C-phased Dy_2O_3 using DFT-PP-WCGGA scheme. The trend of the energy bands computed using DFT-PP-LDA, DFT-PP-PBEsol, DFT-PP-SOGGA and PP-B3LYP is almost similar to those of DFT-PP-WCGGA scheme, and hence the bands only for DFT-PP-WCGGA approximation have been shown. The energy bands confirm a wide indirect band gap of Dy_2O_3. The band structure computed in the present work is in good agreement with that of Horoz *et al.*[11].

The DOS just below the E_F level (Fig. 1(b)), i.e., the valence band in the range −2.9 eV to E_F are due the hybridization of 2*sp* states of O atoms and 5*d* states of the Dy atoms with dominancy of O atoms. In the energy range above 4.60 eV the electronic states are mainly due to the 5*d* states of Dy atoms. Therefore, it has been concluded that the large band gap semiconducting properties of Dy_2O_3 are formed due to positioning of 2*sp* states of O and 5*d* states of Dy atoms. In Table 2, the computed band gaps along with the available data have collated. From this table, it is conferred that DFT based computations (LDA and GGA) of this study are comparable to other reported theoretical data and less than the experimental value[21], whereas the hybrid approach, i.e., B3LYP scheme gives overestimated value of band gap.

Table 1 — Different exchange and correlation potential functions used in present calculations

Theory	Exchange	Correlation
DFT–LDA	Dirac-Slater[23,24]	Perdew–Zunger[25]
DFT–GGA	WCGGA[26]	PBE[27]
	PBEsol[28]	PBEsol[28]
SOGGA	SOGGA[29]	PBE[27]
B3LYP	Becke[30]	LYP[31]

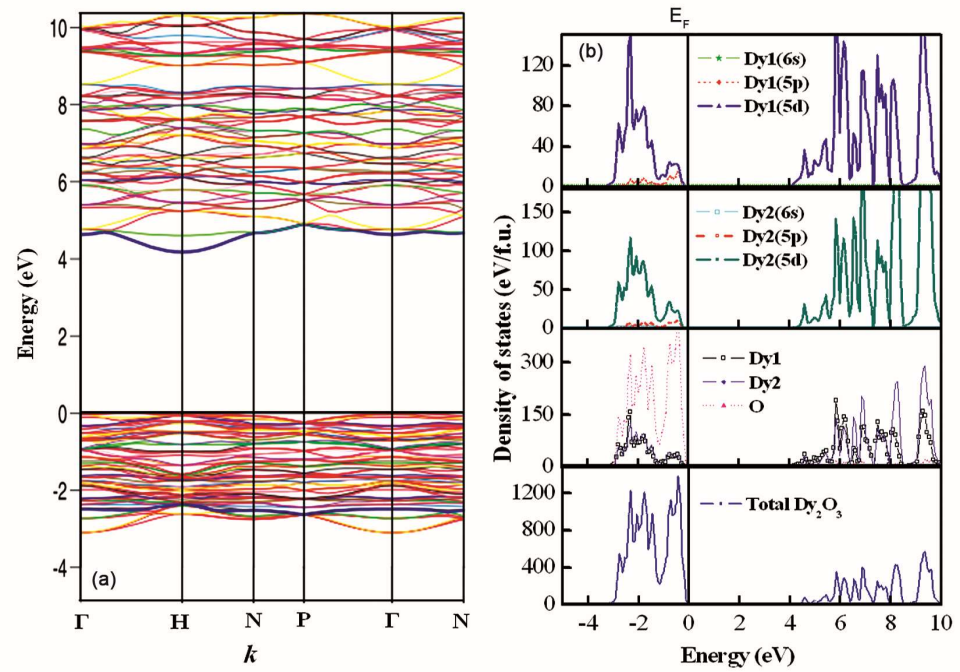

Fig. 1 — (a) Energy bands of cubic Dy_2O_3 along the high symmetry directions and (b) total and partial density of states using DFT- PP-WCGGA scheme.

Table 2 — Energy band gap E_g, for Dy_2O_3 calculated using the various first principle methods along with the available data

Present work		Available work	
Approach	Band gap (eV)	Approach	Band gap (eV)
(a) DFT -PP-LDA	4.09 eV	GGA	3.9[a]
(b) DFT- PP-SOGGA	4.16 eV	HSE03, HSE06	4.7[b], 4.9 [b]
(c) DFT- PP-WCGGA	4.17 eV	LDA+U, G_0W_0, GW_0	3.47[c], 4.41[c], 4.24[c]
(d) DFT- PP-PBEsol	4.18 eV	Experiment	4.9[d]
(e) PP-B3LYP	6.05 eV	(Photo Absorption)	

[a]Ref.[11], [b]Ref.[13], [c]Ref.[15], [d]Ref.[21]

3.2 Compton profiles

The isotropic theoretical valence CPs of Dy_2O_3 deduced from the DFT-PP-LDA, DFT-PP-SOGGA, DFT-PP-WCGGA and DFT-PP-PBEsol schemes are presented in Table 3 and are plotted in Fig. 2. It is seen that near $p_z = 0$, the valence CPs of DFT-PP-WCGGA is higher than DFT-PP-PBEsol /LDA/SOGGA and after 3.0 a.u. all the theories give same values. In Fig. 3, the anisotropies in momentum densities (J_{111}-J_{100}, J_{111}-J_{110} and J_{100}-J_{110}) for Dy_2O_3 have been plotted using DFT-PP-LDA, DFT-PP-SOGGA, DFT-PP-WCGGA and DFT-PP-PBEsol schemes. In this figure, we can see negligible difference in the anisotropies in the high momentum side ($p_z \geq 3$ a.u.) in all the chosen pairs. Such trend is understandable because the high momentum region is dominated by core electrons whose isotropic contributions are cancelled while taking the directional differences. Further, in the low momentum region, small amplitudes of anisotropies $\Delta J(p_z)$ depict a small anisotropic nature of electron density in Dy_2O_3. It is observed that the general trends of oscillations in the anisotropies (Fig. 3) from different schemes are almost identical. The value of anisotropies J_{111}-J_{100} at p_z=0 is higher than J_{111}-J_{110} which shows the higher value of EMD along [110] as compared to [100] at Γ point of BZ.

Further, the oscillations in anisotropies can be related to degenerate states in energy bands and their cross-over near E_F. For example, anisotropies in J_{100}–J_{110} direction can be explained on the basis of degenerate states in Γ–N [100] and Γ–H [110] branches. In Γ–H [110] branch more degenerate states at Γ point are responsible for higher momentum densities in Γ-H branch as compared to Γ-N branch. This leads to positive amplitude of J_{100}–J_{110} in the low momentum region. Also, the positive amplitude in J_{100}–J_{110} near the p_z = 0.7 a.u. arise from the zone boundary of the Γ-N branch (0.77 a.u.). In similar way, we can also explain the other positive and negative anisotropies in different directions.

Theoretical CPs of La_2O_3, Sm_2O_3 and Dy_2O_3 using DFT-PP-WCGGA approach have been plotted in Fig. 4. The profiles are normalized to the irrespective

Table 3 — Isotropic theoretical valence Compton profiles of Dy_2O_3 deduced from the DFT- PP-LDA, DFT-PP-SOGGA, DFT-PP-WCGGA and DFT-PP-PBEsol schemes

p_z (a.u.)	$J(p_z)$ (e/a.u.)			
	DFT- PP-LDA	DFT- PP-SOGGA	DFT- PP-WCGGA	DFT- PP-PBEsol
0.0	16.996	16.976	16.958	16.951
0.1	16.921	16.901	16.883	16.876
0.2	16.682	16.665	16.648	16.641
0.3	16.2670	16.257	16.240	16.233
0.4	15.687	15.678	15.662	15.655
0.5	14.945	14.940	14.926	14.919
0.6	14.044	14.043	14.031	14.023
0.7	12.983	12.987	12.977	12.969
0.8	11.781	11.790	11.783	11.774
1.0	9.136	9.153	9.152	9.142
1.2	6.513	6.533	6.537	6.526
1.4	4.324	4.340	4.346	4.335
1.6	2.805	2.813	2.821	2.810
1.8	1.860	1.862	1.870	1.860
2.0	1.283	1.282	1.288	1.280
3.0	0.309	0.305	0.308	0.305
4.0	0.117	0.116	0.117	0.116
5.0	0.050	0.050	0.050	0.049
6.0	0.023	0.023	0.023	0.023
7.0	0.013	0.012	0.012	0.012

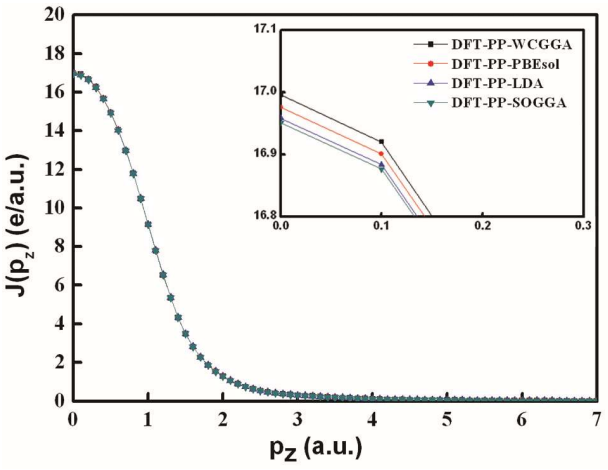

Fig. 2 — Isotropic valence Compton profiles of Dy_2O_3 using DFT-PP-LDA, DFT-PP- SOGGA, DFT-PP-WCGGA and DFT-PP-PBEsol schemes.

free atom CP area in the momentum range 0-7 a.u. (CP data for La_2O_3 and Sm_2O_3 are taken from Sharma *et al* [34,35]). The value of $J(p_z)$ increases when we move from $La_2O_3 \rightarrow Sm_2O_3 \rightarrow Dy_2O_3$ at $p_z = 0$ a.u. The differences in $J(p_z)$ of all the sesquioxides in the higher momentum side ($p_z \geq 3$ a.u.) is found to be very small, which indicates a similar type of behavior of core electrons in these sesquioxides, because this region is mainly dominated by the core electrons. To check a relative influence of 5*d* electrons of La, Sm and Dy in formation of electronic properties of these compounds, we have normalized isotropic theoretical CP of Ln_2O_3

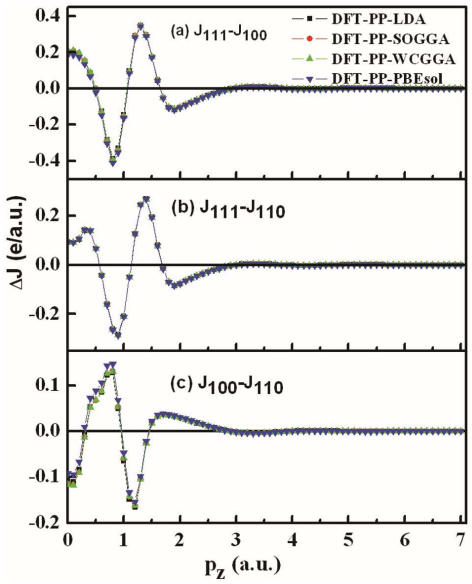

Fig. 3 — (Color online) Anisotropy in the convoluted theoretical Compton profiles of Dy_2O_3 calculated using different density functional schemes within the effective pseudo-core potential. Since the statistical error ±σ is within the size of symbols used, it is not clearly visible. The solid lines are drawn to guide the eyes.

(Ln = La, Sm and Dy) to the same area, viz., free atom area of CP of La_2O_3. From equally normalised (EN) profiles (Fig. 4(b)) it is observed that the trend of EN $J(p_z)$ of La_2O_3 and Sm_2O_3 are almost identical. EN $J(p_z)$ of both La amd Sm sesquioxides differ from that of Dy_2O_3 which may be due to similar type of localization of La-5*d* and Sm-5*d* electrons in their sesquioxides.

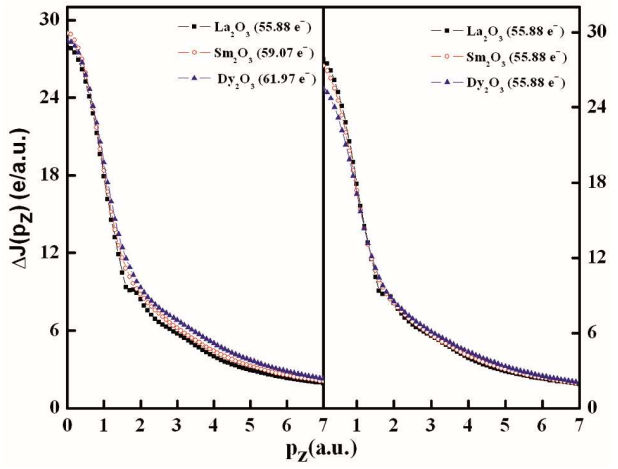

Fig. 4 — (a) Absolute theoretical Compton profile (CP) of La_2O_3, Sm_2O_3 and Dy_2O_3 normalized to the individual free atom (FA) area in the momentum range 0-7 a.u. and (b) CPs of La_2O_3 , Sm_2O_3 and Dy_2O_3 normalized to same area (55.88 e^- of FA area of La_2O_3 in the momentum region 0-7 a.u.). The solid lines are drawn for a quick visibility of the trend.

Table 4 — The Mulliken's population (MP) charge transfer data from donor atoms (Dy1, Dy2) to the acceptor atoms (O) in Dy_2O_3 using the different combinations of exchange and correlation energies (DFT-PP-WCGGA, DFT-PP-LDA and DFT-SOGGA) schemes

Method	Valence charge e^-		
	Dy(1)	Dy(2)	O
PP-DFT-WCGGA	1.776	1.760	-1.176
PP-DFT-LDA	1.762	1.746	-1.166
PP-DFT-SOGGA	1.759	1.744	-1.165
PP-DFT-PBEsol	1.761	1.745	-1.166

3.3 Mulliken's population analysis

In Dy_2O_3, Dy1 and Dy2 play the role of donor atoms while the oxygen atoms play the role of acceptor atoms. Table 4 depicts that charge transfer (total) from donor to acceptor in Dy_2O_3 is 3.503 e^- for PP-DFT-WCGGA scheme, while the values using PP-DFT-LDA, PP-DFT-SOGGGA and PP-DFT-PBEsol schemes are 3.536, 3.508 and 3.506e^-, respectively. Almost similar amount of charge transfer by Dy1/Dy2 to oxygen atoms in Dy_2O_3 is observed. It is seen that the charge transfer from the rare earth elements is equally distributed among the three oxygen atoms.

4 Conclusions

The present work deals with the first ever theoretical momentum density calculations of Dy_2O_3. In this study, we have presented a systematic investigation of electronic properties of cubic Dy_2O_3 crystal using different exchange-correlation functional as prescribed in linear combination of atomic orbitals method. The performance of DFT-PP-LDA, DFT-PP-PBEsol and DFT-PP-SOGGA approaches has been analyzed in probing the electronic properties. Also, the PP-B3LYP hybrid functional has been used to find the energy band gap of the compound.

The energy band gap is an important property that determines the electrical and optical characteristics of the material. It was found that the sample studied has indirect wide band gap of 4.16 eV at room temperature using DFT-PP-SOGGA theory. However, a high dielectric constant is usually accompanied by weaker bonding, suggesting a smaller band gap. But, Dy_2O_3 has high dielectric constant with large value of band gap making it successful to use as insulator between the layers, gate oxide in CMOS and MOSFET devices.

As compared to SiO_2, dysprosium sesquioxide (Dy_2O_3) have high resistivity, dielectric constant, large band gap, recrystallization temperature and thermodynamically stable in contact with Si substrate at high temperature about 800 °C under high vacuum. To overcome the leakage current issue of ultra-thin SiO_2, high–k materials such as rare earth oxides can be chosen as alternative gate insulators.

Acknowledgement

The authors are thankful to the group of Prof R Dovesi for providing the CRYSTAL09 code.

References

1 Ganduglia-Pirovano M V, Hofmann A & Sauer J, *Surf Sci Reps*, 62 (2007) 219.
2 Yang H, Wang H, Luo H M, Feldmann D M, Dowden P C, DePaula R F & Jia Q X, *Appl Phys Lett*, 92 (2008) 062905.
3 Shalini K & Shivashankar S A, *Bull Mater Sci*, 28 (2005) 49.
4 AfanasŠev V V, Stesmans A, Zhao C, Caymax M, Heeg T, Schubert J, Jia Y, Schlom D G & Lucovsky G, *Appl Phys Lett*, 85 (2004) 5917.
5 Fanciulli M & Scarel G, *Rare earth oxide thin film: Growth, characterization, and applications*, (Springer: Berlin), 2007.
6 Frank G, Tatsuro W & Wolfgang B, *Thin Solid Films*, 518 (2010) 4747.
7 Jianjun W, Ting J, Yanyan Z, Zebo F & Weiyi R, *J Rare Earths*, 30 (2012) 233.
8 Adachi G, Imanaka N & Kang Z C, *Binary rare earth oxides*, (New York: Kluwer Academic Publishers), 2004.
9 *Gerald L, Appl Surf Sci, 253 (2006) 311.*
10 *Han X L, Sun M J & Chen S G, J Supercond Nov Magn,* 29 (2016) 2019.
11 Horoz S, Simsek S, Palaz S, Mamedov A M & Ozabay E, *Int J Sci Technol Res*, 1 (2015) 4.
12 Chandrasekhar M, Nagabhushana H, Sudheerkumar K H & Dhananjaya N, *Mater Res Bull*, 55 (2014) 237.
13 Gillen R, Clark S J & Robertson J, *Phys Rev B*, 87 (2013) 125116.
14 Zelati A, Amirabadizadeh A, Kompany A, Salamati H & Sonier J, *Indian J Sci Technol*, 6 (2013) 5552.

15 Jiang H, Rinke P & Scheffler M, *Phys Rev B*, 86 (2012) 125115.
16 Rammo N N, *Iraqi J Sci*, 53 (2012) 316.
17 Dilawar N, Mehrotra S, Varandani D, Kumaraswamy B V, Haldar S K & Bandyopadhyay A K, *Mater Characterization*, 59 (2008) 462.
18 Chiu F C, *J Appl Phys*, 102 (2007) 044116.
19 Petit L, Svane A, Szotek Z & Temmerman W M, *Phys Rev B*, 72 (2005) 205118.
20 Medenbach O, Dettmar D, Shannon R D, Fischer R X & Yen W M, *J Opt A: Pure Appl Opt*, 3 (2001) 174.
21 Prokofiev A V, Shelykh A I & Melekh B T, *J Alloys Comp*, 242 **(**1996) 41.
22 Sugunan S, Sherly K B & Rani D, *React Kinet Catal L*, 52 (1993) 525.
23 Dovesi R, Saunders V R, Roetti C, Orlando R, Zicovich-Wilson M, Pascale F, Civalleri B, Doll K, Harrison N M, Bush I J, D'Arco Ph & Llunell M, *2009 CRYSTAL09 Users' Manual*, (University of Torino: Torino), 2009.
24 Towler M D, Zupan A & Causa M, *Phys Commun*, 98 (1996) 181.
25 Perdew J P & Zunger A, *Phys Rev B*, 23 (1981) 5048.
26 Wu Z & Cohen R E, *Phys Rev B*, 73 (2006) 235116.
27 Perdew J P, Burke K & Ernzerhof M, *Phys Rev Lett*, 77 (1996) 3865.
28 Perdew J P, Ruzsinszky A, Csonka G I, Vydrov O A, Scuseria G E, Constantin L A, Zhou X & Burke K, *Phys Rev Lett*, 100 (2008) 136406.
29 Zhao Y & Truhlar D G, *J Chem Phys*, 128 (2008) 184109.
30 Becke A D, *Phys Rev A*, 38 (1988) 3098.
31 Lee C, Yang W & Parr R G, *Phys Rev B*, 37 (1988) 785.
32 http://www.theochem.uni-stuttgart.de/pseudopotentials/index.en.html
33 http://www.tcm.phy.cam.ac.uk/mdt26/basis_sets /O_basis.txt
34 Sharma S, Sahariya J, Arora G & Ahuja B L, *Physica B*, 450 (2014) 25.
35 Sharma S, Heda N L, Suthar K K, Bhatt S, Sharma K & Ahuja B L, *Comput Mater Sci*, 104 (2015) 205.